Carbon 159 (2020) 102–109

Contents lists available at ScienceDirect

Carbon

journal homepage: www.elsevier.com/locate/carbon

Induced magnetism in oxygen-decorated N-doped graphene

Carlos Romero-Muñiz [a, *, 1], Pablo Pou [a, b], Rubén Pérez [a, b]

[a] Departamento de Física Teórica de la Materia Condensada, Universidad Autónoma de Madrid, E-28049, Madrid, Spain
[b] Condensed Matter Physics Center (IFIMAC), Universidad Autónoma de Madrid, E-28049, Madrid, Spain

ARTICLE INFO

Article history:
Received 13 October 2019
Received in revised form
26 November 2019
Accepted 4 December 2019
Available online 9 December 2019

Keywords:
graphene
Nitrogen doping
Nanopatterning
Induced magnetism
Density functional theory
Covalent functionalization

ABSTRACT

Covalent functionalization of two-dimensional materials is a versatile tool to induce deep changes in their initial properties leading to new functionalities. Unfortunately, in the case of graphene its poor chemical reactivity turns this task rather difficult from the practical point of view. In this work, we show how the adsorption of external species can be controlled by substitutional nitrogen atoms properly distributed through the graphene layer. Nitrogen atoms can be experimentally incorporated in the graphene lattice with high precision and tunable concentration and they can be used as active sites to trigger an ordered functionalization. By means of first-principles calculations we study the adsorption of single and multiple oxygen atoms in the vicinity of substitutional N defects, revealing a rich scenario regarding adsorption configurations and electronic properties. In particular, we find a stable structure involving three oxygen atoms that induces a robust magnetic behavior in the graphene layer. The great chemical variability found in the oxygen-decorated N-doped structures presented in this study constitutes a valuable platform for the future development of graphene-based electronic and sensing devices.

1. Introduction

In the last years, the research work focused on graphene functionalization has attracted increasing attention [1]. The reason for such interest is related to expand the capabilities of graphene for further applications. Despite its great promising properties, it is well-known that free-standing graphene lacks of an electronic band gap and displays a poor chemical reactivity. This circumstance weakens the competitive strength of graphene in the fields of semiconductors and sensors. In order to overcome these issues, different strategies have been developed to promote chemical reactions of graphene (both with organic and inorganic molecules) with the final aim of producing covalent patterns on graphene interfaces with the desired properties. However, the chemical inertness of graphene makes rather difficult a controlled and selective covalent functionalization. Recent attempts have taken advantage of the remarkable chemical reactivity induced by defects [2–4] or even the rippled structure adopted by the graphene layer grown on transition metal substrates [5–10]. In spite of the technical difficulties found in the experimental side, these functionalization approaches have proven to be highly beneficial, providing new features to the graphene layer, like a band gap opening via hydrogenation [6,11] or diazonium compounds reactions [12]. Of course, these techniques are not exclusively restricted to graphene, but they can be applied to other bidimensional materials [13,14].

The search for magnetic behavior in graphene and other 2D materials is another topic of special relevance in which covalent functionalization can be useful [15]. Graphene itself does not show a magnetic behavior but it is possible to confer some magnetic moment either through the interaction with a ferromagnetic substrate like nickel, or cobalt [16–19], with the aid of transition metal atoms [20], or via single-atom vacancies engineering [21–23], what has been studied in depth in the literature [21,22,24–29]. Lastly, theoretical studies suggested that it was possible to induce a magnetic moment through chemical modification using different species [30–32]. Recent scanning tunneling microscopy experiments [33] have demonstrated this point, revealing that a covalent functionalization based on the controlled adsorption of hydrogen atoms is indeed a suitable alternative for this purpose. In any case, we have to take into account the remarkable experimental difficulties to control the addition of defects with sufficient order, which has been reported to be an essential aspect to retain the induced magnetic properties on the layer. For instance, point defects too close to each other belonging to different sublattices could

* Corresponding author.
E-mail addresses: carlos.romero@uam.es (C. Romero-Muñiz), pablo.pou@uam.es (P. Pou), ruben.perez@uam.es (R. Pérez).
[1] Present address: Department of Physical, Chemical and Natural Systems, Universidad Pablo de Olavide, Ctra. Utrera Km. 1, E–41013, Seville, Spain.

https://doi.org/10.1016/j.carbon.2019.12.007
0008-6223/

turn off the magnetism [28,33]

Heteroatom dopants, as any other point defects, break the lattice symmetry conferring to the surrounding areas distinctive properties different from those observed in pristine graphene. In particular, the incorporation of substitutional –referred also as graphitic– nitrogen atoms in the graphene lattice leads to an enhancement of the chemical reactivity, making feasible the use of N-doped graphene as a metal-free catalyst for a number of chemical reactions [34–38]. Besides, unlike other kinds of point defects, recent progress in the production techniques enables the synthesis of high quality samples with tunable concentration on different substrates [39–43]. Even, in nanoribbons, on-surface synthesis has allowed the controlled addition of different atoms with atomic precision [44–46]. Moreover, nitrogen atoms are able to tune the interaction with external species [47], and hence, can be used as active centers for further functionalization, as it has been recently demonstrated [48].

In this work, we investigate the potential applications of substitutional nitrogen atoms to induce further chemical modifications, showing a remarkable variation of the electronic properties depending on the interactions with the bounded species. For this purpose, we study in detail the behavior of nitrogen substitutional defects in the presence of atomic oxygen adsorbates, and how they affect the electronic properties of the graphene layer. We perform Density Functional Theory (DFT) calculations on N-doped graphene with one or more oxygen atoms adsorbed on the neighborhood of the nitrogen defect. Firstly, we focus on the adsorption of a single oxygen atom near the nitrogen defect, previously considered by other authors focused on catalysis [38,49–51]. We confirm how the chemical reactivity of the system is enhanced in the vicinity of the defect and how adsorption configurations differ from those found in undoped graphene. Additionally, we study the adsorption of multiple oxygen atoms revealing strong interactions between adsorbates. Finally, we study the electronic properties of the graphene layer that can be drastically modified depending on the adsorption configuration of the oxygen atoms. Moreover, we show that a structure containing three oxygen atoms surrounding the N-center induces a magnetic moment of 1 μ_B in the graphene layer. The high stability of this structure suggests that it could be experimentally achieved.

Combining the controlled oxygen adsorption with the possibility of designing periodical arrays of N-doped (or other heteroatoms) graphene layers, as it is indeed possible for nanoribbons [44–46], would allow us to tune their magnetic properties, preventing the quenching of the magnetism that appears in disordered distributions of point defects [28,33]. Thus, our work shows that subtle chemical modifications on N-doped graphene provoked by oxygen adsorbates leads to a great variability of its electronic properties which promotes new opportunities to the design of electronic devices.

2. Computational details

Our theoretical approach is based on DFT calculations using the plane-wave basis code VASP [52] with a cutoff of 400 eV for the basis set. Pseudopotentials for all species (C, N and O) were built using the projector augmented wave method [53,54]. A Generalized Gradient Approximation (GGA) was used for the exchange and correlation functional as described by Perdew, Burke and Ernzerhof (PBE-functional) [55] supplemented by the D2 semi-empirical correction [56] to take into account dispersion forces.

We have constructed our graphene cell using a lattice parameter of 2.4678 Å, obtained by DFT simulations, corresponding to a C–C bond length of 1.4248 Å. These values are very close to their experimental counterparts, 2.4595 Å and 1.42 Å respectively [57]. Periodic boundary conditions are used in the simulations with different unit cells. Most of the calculations are performed on a $[(\sqrt{43}\times\sqrt{43})-R7.6^\circ]$ unit cell which contains 86 C atoms. One of the C atoms was replaced by a N atom and several structures involving one, two or three oxygen atoms were studied. This rhombic cell has a side of 16.18 Å and more than 20 Å of vertical spacing are left between periodical images along the z axis. This choice allows us to perform reliable calculations on a large enough unit cell but keeping reasonable computational requirements. In any case, we have analyzed other cells, i.e. (4×4), (5×5), (8×8) and (10×10) in order to study the influence of defect concentration. Adsorption energies per oxygen atom are calculated as usual:

$$E_{ad} = \frac{E[\mathrm{tot}] - E[\mathrm{G}] - N_O E[\mathrm{O}]}{N_O}, \quad (1)$$

where N_O is the number of adsorbed oxygen atoms, E[tot] is the energy of the total system including graphene plus oxygen atoms, and E[G] and E[O] are the energies of the isolated N-doped graphene layer and one oxygen atom respectively. Thus, we have considered the isolated oxygen atom as reference instead of the O_2 molecule. To convert our results to the ones using the molecular state as reference we can simply shift the chemical potential by 3.05 eV, which is half of the dissociation energy of the molecule. However, this value is poorly estimated at the GGA level compared to the experimental figure of 2.56 eV [58].

All structures were subjected to ionic relaxations following a conjugate gradient algorithm until forces upon atoms were less than 0.01 eV/Å. During these relaxations all atoms were allowed to relax. The reciprocal space was sampled using a $2\times2\times1$ Monkhorst-Pack grid [59] during the structural relaxations in the $[(\sqrt{43}\times\sqrt{43})-R7.6^\circ]$ cell while different meshes were used in other cells according to their sizes. A thinner grid of $11\times11\times1$ was employed for electronic structure calculations in all cases except in the structure containing three oxygen atoms where a $31\times31\times1$ grid was used to characterize accurately the electronic properties like the spin-resolved density of states. In all cases, spin-polarized calculations were carried out for all structures in the search of magnetic ordering. In non-magnetic cases we use a Gaussian smearing of 0.1 eV while for the three-oxygen-atom structure, where the magnetic moment is stabilized, we study the evolution of the magnetization as a function of the electronic temperature in the range $0.01-0.1$ eV. Further tests with the Methfessel-Paxton smearing [60] were carried out without finding any remarkable difference in the final results.

The charge transfer between oxygen atoms and the N-doped graphene layer was evaluated using Bader analysis, following the algorithm developed and implemented by Henkemnan's group [61–63]. Finally, theoretical Scanning Tunneling Microscopy (STM) images for different bias voltages were obtained from the local density of states using the Tersoff-Hamann approximation [64,65] and processed with the WSxM software [66].

3. Results and discussion

3.1. Adsorption of atomic oxygen on N-doped graphene

The adsorption of atomic oxygen on free-standing graphene has been already studied, revealing that oxygen atoms preferentially adsorbs on bridge positions forming epoxy groups [67,68]. In this work, we show that substitutional nitrogen defects represent an additional way to substantially modify the predominant trends observed in free-standing graphene.

Fig. 1 shows a selection of three different adsorption configurations involving one single oxygen atom depending on the

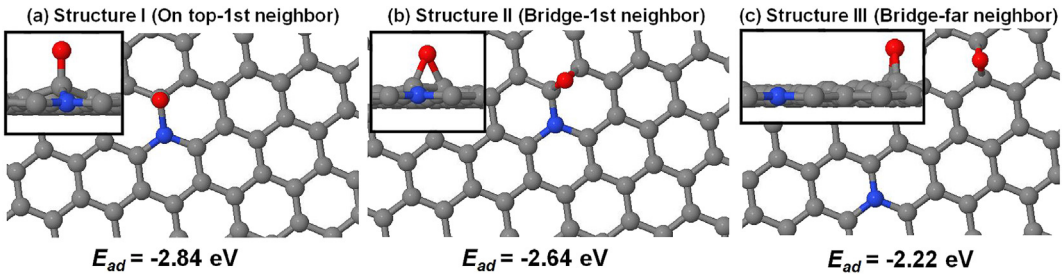

Fig. 1. Schematic representations of several structures of one oxygen atom adsorbed on a N-doped graphene layer. (a) Adsorbed on top of a first neighbor carbon atom. (b) Adsorbed on bridge positions between a first and a second neighbor. (c) Adsorption on bridge position far from the defect, similarly to the undoped case. (A colour version of this figure can be viewed online.)

distance to the N-center. The most energetically favorable adsorption site is on top of a nearest neighbor carbon atom. It is worth mentioning that our calculations discard other configurations with the oxygen atom even closer to the nitrogen defect. For example, the oxygen adsorption directly on top of the N-center is not a stable configuration. The most stable configuration, labeled as structure I, is shown in Fig. 1a and its adsorption energy is − 2.84 eV. If we move away from the defect, bridge positions become again stable but showing higher energetic configurations with increasing distance. For instance, a bridge configuration near the nitrogen atom (structure II) is shown in Fig. 1b, whose adsorption energy, − 2.64 eV, is slightly less attractive. Finally, for large enough distances the adsorption takes place exactly in the same way as in pristine graphene (structure III), see Fig. 1c. However, this configuration is clearly less energetically favorable, with an adsorption energy of − 2.22 eV. Notice that this value is very close to our calculated oxygen adsorption energy in the undoped graphene (− 2.17 eV), which is in agreement with a number of previous calculations [68–70]. Thus, an increment of ∼ 0.7 eV (> 30%) on the adsorption energy is gained due to the presence of the nitrogen atom. We remark that bridge positions are the only ones stable throughout the N-doped graphene layer except for the on-top configuration near the N-center already described. The adsorption energies of these configurations decrease as we increase the distance from the N defect, following the expected energetic landscape.

From the structural point of view, the adsorption of oxygen on free-standing graphene always induces some corrugation due to the change on the hybridization state of bonded carbon atoms [71]. While the structural parameters in the bridge position are compatible with the geometry of an epoxy group, in the C-top adsorption, the most favorable configuration, the C atom just below the adsorbed oxygen atom changes its hybridization state to an sp^3 configuration as demonstrated by its tetrahedral angles. In particular their values for the equilibrium geometry of structure I are 109.2°, 108.4° *and* 109.4° The C–O bond presents a length of 1.32 Å revealing a partial double bond character. These structural features are in agreement with previous studies [49,50] and supported by our Bader charges analysis, which points out a larger charge accumulation (0.2*e*) in those oxygen atoms adsorbed on-top with respect to those on bridge configurations.

Note that the increment of the chemical reactivity produced by graphitic dopants relies on the extra charge provided by the N atom to the π-states close to the Fermi level of the neighbouring carbon atoms [39,41], which can be used to form the new oxygen-carbon covalent bond. Thus, the ultimate effect of the nitrogen dopant is an effective energy reduction between the sp^2 and sp^3 hybridization states of the neighbouring C atoms, leading to the hybridization change in the presence of a reactive species like atomic oxygen. Therefore, the modification of the adsorption sites for atomic oxygen is a proof of the enhancement of the chemical reactivity induced by substitutional nitrogen dopants. This situation is similar to the one reported recently for graphene grown on strongly interacting metallic substrates, where a local enhancement of the chemical reactivity has been also observed [10]. This is due to the strong interaction with the substrate, which promotes the change of the hybridization states of some carbon atoms.

Now, we move to analyze what happens when more than a single oxygen atom is involved in the adsorption process. Since we have demonstrated the preference of oxygen atoms to adsorb close to the nitrogen defect, we are going to restrict to the multiple adsorption near the nitrogen defect exclusively, as illustrated in Fig. 2. Note that the adsorption of a single atom in Fig. 2a, is the structure I discussed before. An oxygen atom adsorbed on top of a nearest neighbor carbon atom, which resulted the most energetically favorable configuration in the single-atom case. When two oxygen atoms are adsorbed at the same time the simultaneous occupancy of top configurations is not allowed. As a result, one of them remains on top, exactly as in the single-atom case, while the second atom adopts a bridge configuration typical of undoped graphene, see Fig. 2b. This situation indicates that there is not enough available charge on the vicinity of the defect to create two C–O bonds with the characteristics of the partially double bond described before. Therefore, the alternative solution is to keep one of these bonds while the other oxygen forms an epoxy group. Finally, if three oxygen atoms are considered, none of them adsorbs on top positions. This fact can be attributed to the repulsion between oxygen atoms, which prevents the occupancy of top positions. As it is shown in Fig. 2c, the final configuration corresponds to three oxygen atoms adsorbed on bridge positions between first and second carbon neighbors, retaining the flatness of the graphene layer. The adsorption energies per oxygen atom of these structures near the N-centers are very stable from the energetic point of view, with adsorption energies similar to the most favorable single-atom configuration, being −2.63 eV and −2.77 eV for two- and three-atom structures respectively. Notice that the number of quasi-equivalent configurations might be degenerate. For example, the configuration represented in Fig. 2c has an almost equivalent chiral structure generated by moving oxygen atoms to the next equivalent bridge position. Other non-equivalent configurations may include possible permutations of one oxygen atom, but these configurations would be less symmetrical and less stable.

3.2. Electronic properties of oxygen-decorated N-centers

In the preceding section we have studied the chemical bonding of oxygen atoms near substitutional nitrogen defects, revealing the existence of a rich chemical scenario. Consequently, a similar situation is expected regarding the electronic properties of these oxygen-decorated structures. In this section, we will disclose them and show that the subtle interplay among adsorbed species gives

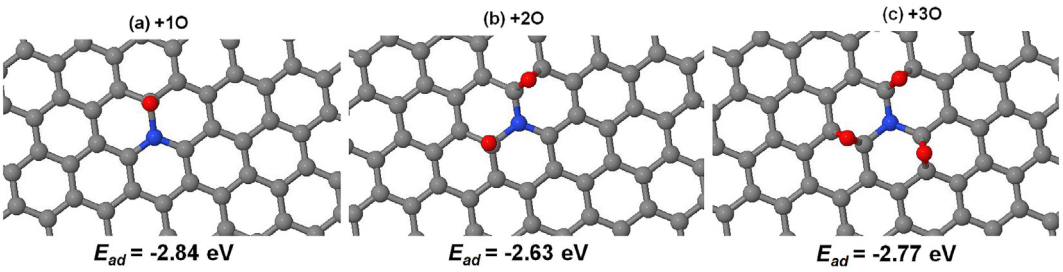

Fig. 2. Schematic representations of several structures containing a different number oxygen atom adsorbed near a substitutional nitrogen atom on a graphene layer. (a) One atom adsorbed on top of the first neighbor carbon atom. (b) Two oxygen atoms adsorbed on top and on bridge sites. (c) Three oxygen atoms adsorbed on bridge positions near the nitrogen defect. (A colour version of this figure can be viewed online.)

rise to highly tunable properties that could be useful for functionalization applications.

Firstly, we analyze the electronic properties of the three single-adsorbate structures I, II and III discussed in the previous section. In the upper panel of Fig. 3, we show the Projected Density of States (PDOS) of the nitrogen and oxygen atoms as well as other relevant carbon atoms (C1, C2, C3 and C4). For structures II and III, where the oxygen bridge configuration is found, the doping level is the same as in the N-doped graphene without oxygen. Conversely, in the structure I, the Dirac cone is abruptly shifted $\sim +1$ eV to the p region (see the differences of the PDOS corresponding to the C4 atom). This is a consequence of the distinctive C–O bond created in this configuration, rather different to the epoxy configurations displayed in structures II and III. In this regard, our Bader charges analysis also predicts a larger charge withdrawn for the unusual C–O bond in structure I ($0.91e$) with respect to epoxy-like arrangements of structures II and III ($0.79e$ and $0.80e$ respectively). Unfortunately, this analysis is unable to discern if this charge comes from the graphene π bands or not. In any case, this point is especially relevant if we take into account the geometrical similitude and the small energy difference of 0.20 eV between structures I and II. This circumstance opens the door to carry out atomic manipulation or even the spontaneous exchange between both structures. Another interesting feature is the low amount of available states in a broad range around the Fermi level in those carbon atoms bonded to oxygen adsorbates compared to other neighbouring atoms. This is a characteristic common to all structures and it is a consequence of the formation of covalent bonds. The PDOS associated with the nitrogen and oxygen atoms is roughly similar in all cases, presenting a peak near the Fermi level. The most significant difference relies on the oxygen atom adsorbed on top, which possesses a remarkably larger PDOS around the Fermi level due to in-plane p-states. It is worth noting that none of these three single-atom structures present a magnetic solution despite having an odd number of electrons. In the next section we will discuss in more detail the reasons responsible for the absence of magnetic behavior.

We have also investigated the theoretical STM contrast of these structures by means of the Tersoff-Hamann approximation. In all cases, the peak in the PDOS displayed by the oxygen atom, together with the evident difference in height, leads to intense bright spots in the STM images. In structure I, the contribution of the oxygen adatom cannot be distinguished from the effect of the nitrogen atom, which apparently preserves the three-fold symmetry. Something similar occurs with structure II, in which the bridge orientation of the oxygen atom can be hardly discerned in the image but, still, both defects are too close to be properly resolved. In structure III, the oxygen adatom is far enough to visualize both defects separately, the oxygen atom adsorbed on bridge position

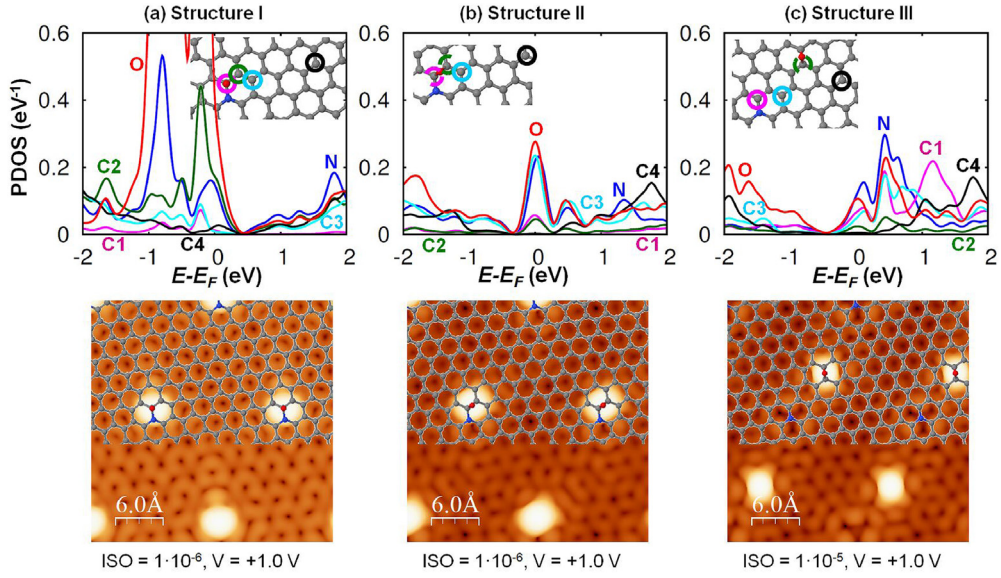

Fig. 3. Electronic structure for three different adsorption configurations of atomic oxygen on N-doped graphene. In each case we show the projected density of states of the N atom, the O atom and some representative carbon atoms (C1, C2, C3, and C4) of N-doped graphene as indicated in the insets. Additionally, each structure if accompanied by the corresponding theoretical STM image after the Tersoff-Hamann formalism (isosurfaces values in $e/\text{Å}^3$). (A colour version of this figure can be viewed online.)

with the same fingerprint of structure II and the nitrogen defect with its typical ternary symmetry described elsewhere [39,41].

Similar to the single-atom adsorption, the upper panel of Fig. 4 summarizes the electronic structure of the system when two oxygen atoms are adsorbed near the substitutional N atom. Now, the essential features displayed by the systems are somehow, a combination between those observed in structures I and II previously introduced. For example, the presence of a partial C–O double bond implies the displacement of the Dirac cone towards the p region, due to the charge withdrawal produced by the oxygen atom. Thus, the p-like contribution arising from the on top adsorption of an oxygen atom, observed in structure I, is confirmed again. On the other hand, the strong oxygen peak observed in structure I has been shifted to lower energies, while the PDOS shape of the N atom is almost identical. The PDOS of those carbon atoms bonded to oxygen atoms remain much smaller than other atoms on a broad range $[-2, +2]$ eV around the Fermi level. The analysis of the STM image (see the lower panel of Fig. 4) using the Tersoff-Hamann approximation is in concordance with those features obtained in the case of a single oxygen atom: Oxygen atoms are visualized as bright spots due to the topography and the accumulation of charge. In this case, the two oxygen atoms can be separately resolved as different spots.

The most surprising scenario appears when three oxygen atoms are symmetrical adsorbed around the N-center. Figs. 5a and b show the PDOS of a number of relevant atoms in the system. As it is seen, the electronic structure of N-center with three bridge adsorbed O atoms in its neighborhood is completely different from all other structures introduced so far in this work. Undoubtedly, the most remarkable feature is the emergence of a magnetic solution. In this multiple adsorption configuration, the pronounced peaks of O and N atoms responsible for the chemical bonding have been shifted to lower energy values with the exception of a sharp state close to the Fermi level, which is only filled with one electron. Therefore, the spin degeneracy is broken, giving rise to an energy splitting between up and down states and a local magnetic moment of $\sim 1\ \mu_B$ per oxygen-decorated N-center. This state is localized on the carbon atoms belonging to one of the sublattices (the one without the N atom), and has also some weight on the oxygen atoms but it is much smaller in the N atom and its three C nearest neighbors. The energy splitting is as large as 310 meV for small N–N distances or high defect concentration (see the 4×4 cell in Table 1) and the it decreases with increasing N–N distance, being 130 meV for the $\sqrt{43} \times \sqrt{43}$–R7.6° cell represented in Fig. 5. This trend is very similar to the one reported for the case of H on graphene [33].

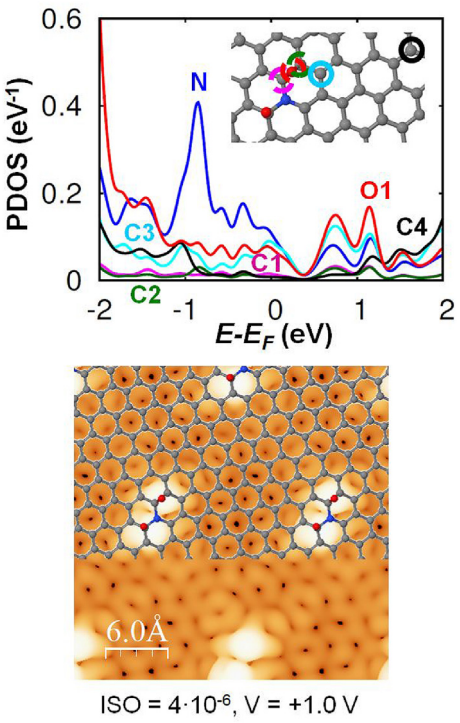

Fig. 4. Electronic structure of two oxygen atoms adsorbed on N-doped graphene. We show the projected density of states of the N atom, one O atom and some representative carbon atoms (C1, C2, C3 and C4) of N-doped graphene as indicated in the inset. In addition, the corresponding theoretical STM image after the Tersoff-Hamann formalism if shown in the lower panel (isosurfaces values in $e/$ Å^3). (A colour version of this figure can be viewed online.)

Another characteristic, clearly observed in the PDOS shown in Figs. 5a and b, is that the sharp peak is embedded in the middle of a band gap of ~ 1 eV. This gap is observed in all the atoms of the simulation cell. This fact is a consequence of the interaction between defects in different cells. Upon reduction of the defect concentration its magnitude is reduced until it starts to vanish at N–N distances larger than 25 Å (i.e. $\sim 0.5\%$ N/C at.). Results of the band gap as function of the cell size (or defect concentration) are shown in Table 1, revealing that its width strongly depends on the defect concentration.

Finally, we have presented in Fig. 5d–g the Tersoff-Hamann images of the oxygen adsorbates for different bias voltages. Unlike the two-oxygen case, the overlap among oxygen atoms does not allow us to resolve the different atoms except for high positive voltages (see the 1 V case). For other voltages, a single triangular spot is observed. In addition, the distinctive properties between the two sublattices of graphene is clearly visible for those images at low voltages (see ±0.25 V cases).

3.3. Emergence of magnetism in oxygen decorated N-doped graphene

It is well-known that pristine graphene lacks an intrinsic magnetic behavior. According to Lieb's theorem [72], such a system with an even number of electrons is unable to display any magnetic moment unless an unbalanced situation between both sublattices was achieved. In principle, the presence of further external agents like defects would be necessary for this purpose.

Naively, it can be thought that the introduction in the graphene lattice of heteroatoms with a different number of valence electrons (like nitrogen) could be a straightforward way to induce magnetic behavior in the layer. However, this is not true. In the case of N-doped graphene with concentrations less than $\sim 6\%$ N/C at., a nonmagnetic ground state is expected, as explained by Błoński and coworkers [73] This absence of magnetic behavior is related to the preservation of G π-band upon nitrogen incorporation. The extra electronic charge is stored in lower energetic levels, shifting the Dirac cone and leading uniquely to a remarkable negative doping. Only for higher concentrations it is possible to find weak magnetic solutions ($\ll 1\ \mu_B$), and the description of the magnetism becomes complex and highly dependent on the nitrogen concentration and its geometrical arrangement. Moreover, a large number of possible magnetic configurations can be found with a varying effective magnetic moment per cell and exhibiting ferromagnetic, antiferromagnetic behaviors, or even a lack of magnetic order [73]. A similar scenario has been reported for substitutional sulphur atoms in graphene [74].

The chemisorption of different species on top of C atoms represents a suitable option to induce magnetism in the graphene layer. In particular, this behaviour is found in most of the cases involving a sp^3 -type organic functionalization, where a new covalent bond (C–C or C–H) is created between the graphene and the

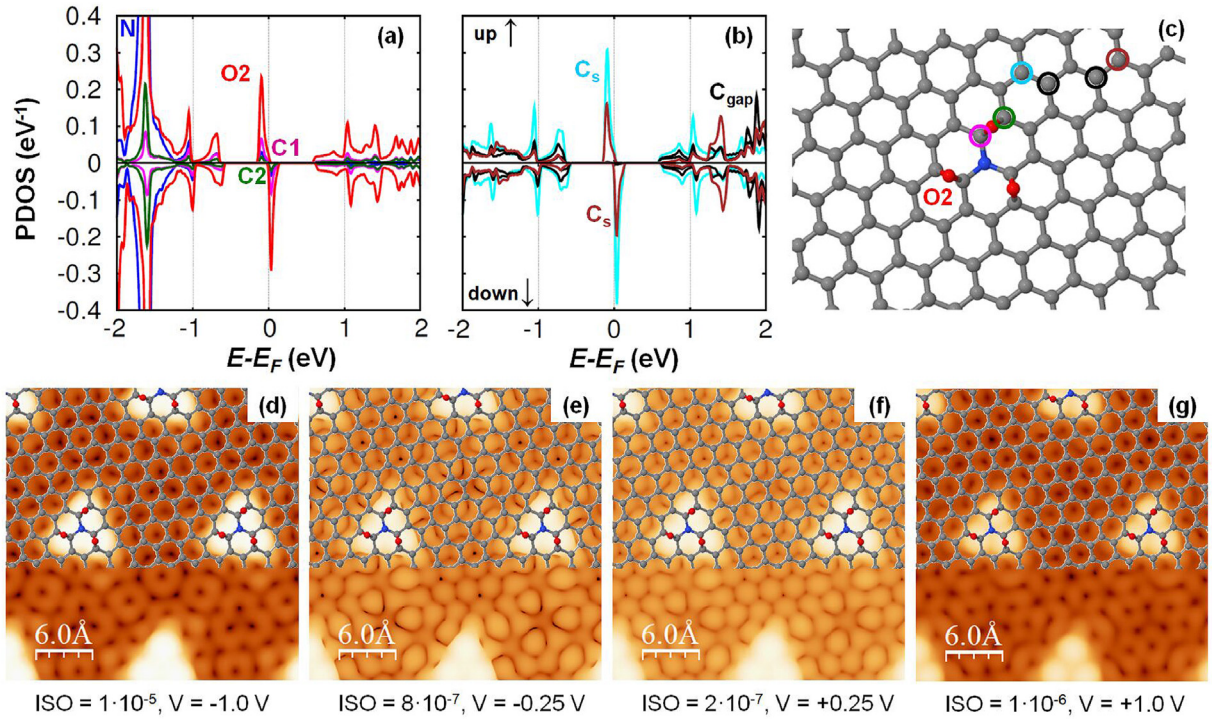

Fig. 5. Electronic structure of three oxygen atoms adsorbed on N-doped graphene. The spin polarized projected density of states of some atoms is shown in (a) and (b). We include the N atom, one O atom and two carbon atoms (C1 and C2) in (a) and some additional carbon atoms in (b), as indicated in (c). In this latter case two different species are found, C_s *and* C_{gap}, displaying a split state and a band gap respectively. Theoretical STM images (isosurfaces values in $e/Å^3$) after the Tersoff-Hamann formalism have been included for different voltages (d–g). In order to capture this magnetic behavior properly, a low electronic temperature must be used in the calculation, for example $\sigma = 0.02$ eV and a very dense *k*-point mesh has been used to resolve the sharp peaks of the PDOS, as specified in the method section. (A colour version of this figure can be viewed online.)

Table 1
Characteristics of the unit cells used to determine the local influence of the N substitutional defects in the graphene lattice. The band gap width is calculated from the PDOS of selected C atoms.

cell	Area	N–N dist.	N/C	Density	Band gap width
	(nm^2)	(Å)	(% at.)	(nm^{-2})	(eV)
4 × 4	0.844	9.87	3.13	1.185	1.77
5 × 5	1.319	12.34	2.00	0.758	1.61
$\sqrt{43} \times \sqrt{43}$–R7.6°	2.266	16.18	1.16	0.441	1.10
8 × 8	3.376	19.74	0.78	0.296	0.88
10 × 10	5.274	24.68	0.50	0.190	0.56

adsorbate [30,33]. This kind of organic functionalization leads to a magnetic moment of 1 μ_B because one electron is removed from the π-band and retained in the covalent bond, creating a semi-localized state in the neighbouring carbon atoms. However, strong polar species, such as fluorine or other halogens, adsorbed on graphene do not cause the same effect [30,31,75,76]. This is due to the absence of truly covalent bonds in favor of a remarkable ionic contribution [30,31]. Besides, in this latter case, the situation becomes more complex because the higher electronegativity of the absorbate may affect the doping level importantly. It has been shown that the doping level is able to switch on and off the magnetic moments of the graphene layer [23]. As a result, it is much more complicated to stabilize the magnetic moment using electronegative atoms, at least for low adsorbate densities [31,75,76].

In the case of single oxygen atoms adsorbed on pristine graphene, we have to take into account that it adsorbs necessarily on bridge position. Therefore it will be impossible to induce magnetic behavior in the layer because the two new bonds are created in different sublattices and, in any case, an even number of electrons is preserved in the π-band. Thus, the possibility of generating the unbalance between sublattices required to induce the magnetic moment is discarded. In N-doped graphene, the presence of substituional N-centers makes possible the O adsorption on top position, as we have already explained (see structure I). However, this feature is not sufficient to provoke the emergence of the magnetic moment due to the high electronegativity of atomic oxygen. In this sense, oxygen atoms behave similarly to the case of fluorine and other halogens, at least at low concentrations. If we consider two oxygen atoms adsorbed near the N-center, the situation remains unchanged since the second atom occupies a bridge position. However, in the three-oxygen N-doped graphene structure reported in Fig. 2c, a magnetic moment of 1 μ_B is obtained, despite having all adsorbates on bridge positions.

This surprising result arises from a situation rather different with respect to the simpler examples described before. Essentially, the hybridization of the three oxygen atoms forming epoxy groups locally destroys the G π-band in the neighborhood of the N-center leading to its full isolation from the layer and thus, producing the unbalance between sublattices leading to the final magnetic character. The spin charge density landscape is shown in Fig. 6, which is mainly localized throughout the π-bands of the graphene layer constituted by the carbon p_z orbitals. Although the total magnetic moment induced in the layer is 1 μ_B, the spin is distributed all over the layer, revealing the slow decay of the spin moment created by this functionalization [24,33]. The distribution of the spin moment follows the twofold nature of the graphene lattice. The accumulation of spin density on the N-center is negligible and the magnetic moment over the three carbon first-neighbors is also rather low. Conversely, oxygen atoms store up spin together with those C atoms belonging to the N-free sublattice, while the down spin

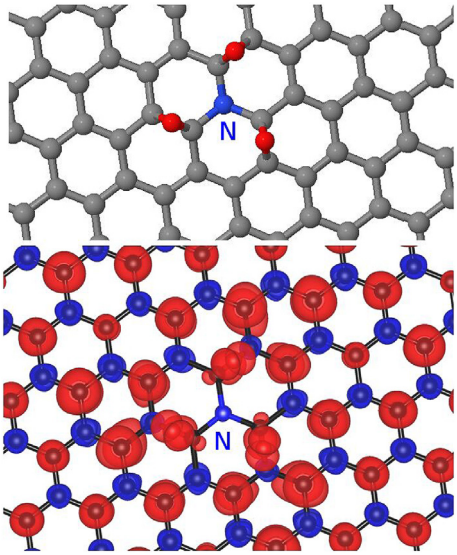

Fig. 6. Spin density in the oxygen-decorated N-doped graphene layer. The original structure is shown in the upper panel while the superimposed spin density is displayed in the lower panel (calculated with a Gaussian smearing of 0.02 eV). In both cases the N substitutional atom appears in the center. Electron up and down densities are shown in red and blue colors respectively for isodensity values of $\pm 5\times 10^{-4}\ e/\text{Å}^3$. Note the charge splitting between both sublattices, in agreement with the projected density of states. (A colour version of this figure can be viewed online.)

density is retained in the sublattice owning the N-center. This spin distribution is rather similar to those found after direct functionalization with organic adsorbates like CH_3, C_2H_6, COOH, etc. [30] However, this latter proposal is much more difficult to achieve experimentally. On the contrary, oxygen atoms are specially appropriate candidates for this purpose. They are highly reactive species which can diffuse throughout the graphene layer, as demonstrated by experimental work in undoped graphene [77,78]. In addition, the saturation value of 1 μ_B is reached for electronic temperatures up to 0.025 eV, revealing the robust nature of the magnetic behavior and pointing out that it is expected not only for extremely low temperatures.

This overall behavior, the emergence of magnetism and the opening of a band gap at certain defect concentrations, is very similar to the one reported for atomic hydrogen adsorbed on graphene [33]. The difference here is that substitutional N atoms can act as fixing centers to promote an ordered functionalization. This fact would be highly beneficial from the experimental point of view. Remember that the creation of two defects closely located but in different sublattices quenches the magnetism. In the case of the hydrogen adsorption, this is the most energetically favorable configuration [33] making the experimental production of magnetic samples remarkably hard. In this regard, the possibility of growing controlled N-patterned graphene layers [44–46] could avoid this difficulty and open the door to tune the magnetic properties, as well as inducing a band gap with tunable width, on graphene layers.

4. Conclusions

In summary, we have theoretically shown how substituional N-defects embedded in a graphene layer can be used as active sites to control a subsequent covalent functionalization with atomic oxygen. We have investigated in depth the adsorption of atomic oxygen near a graphitic N-defect on free-standing graphene. As a novelty, we pay special attention to the evolution and tunability of the electronic properties upon adsorption. This includes, changes on the electronic doping level, the opening of a band gap, and the emergence of a permanent magnetic moment when three oxygen atoms adsorbed on bridge positions symmetrically surround the N-center. Moreover, we have discussed the feasibility of obtaining these structures experimentally. The local enhancement of the chemical reactivity in the neighborhood of these dopants leads to high values of adsorption energies (−2.77 eV per oxygen atom). Therefore, these findings reveal the suitability of this kind of structures to be experimentally achieved.

The search for exotic electronic properties in two-dimensional materials is attracting much attention due to its potential applications in the development of electronic devices with new functionalities or a better performance. This work moves one step forward in this direction, concluding that a magnetic moment of 1 μ_B can be induced on N-doped graphene when a graphitic N atom is isolated from the graphene π-bands. We have illustrated this effect with the particular choice of oxygen adatoms but this approach could have been carried out with other adsorbates, leading to new interesting properties. Notice that this goal is reached by means of covalent functionalization even without considering any ferromagnetic species. We expect that this study could serve as a platform for future experimental work based on the functionalization proposal presented here.

Author conttibution

CRM, PP and RP conceived and designed the study, collected and analyzed the simulation data. CRM wrote the manuscript with inputs from PP and RP.

Declaration of competing interest

The authors declare no interest of conflicts regarding any financial or personal circumstance that could affect the course of the research or the results presented in this work.

Acknowledgements

We thank the financial support from the Spanish MINECO (AEI/FEDER, UE): projects MAT2014-54484-P, MDM-2014-0377 and MAT2017-83273-R. CRM is grateful to the FPI-UAM graduate scholarship program and to Fundación Universia for financial support. We thank Dr. Ana Martín-Recio and Prof. José María Gómez-Rodríguez for many useful discussions.

References

[1] V. Georgakilas, M. Otyepka, A.B. Bourlinos, V. Chandra, N. Kim, K.C. Kemp, P. Hobza, R. Zboril, K.S. Kim, Chem. Rev. 112 (2012) 6156–6214.
[2] D.W. Boukhvalov, M.I. Katsnelson, Nano Lett. 8 (2008) 4373.
[3] Y. He, M. Garnica, F. Bischoff, J. Ducke, M.-L. Bocquet, M. Batzill, W. Auwärter, J.V. Barth, Nat. Chem. 9 (2016) 33.
[4] R.A. Bueno, J.I. Martínez, R.F. Luccas, N. Ruiz del Árbol, C. Munuera, I. Palacio, F.J. Palomares, K. Lauwaet, S. Thakur, J.M. Baranowski, W. Strupinski, M.F. López, F. Mompean, M. García-Hernández, J.A. Martín-Gago, Nat. Commun. 8 (2017) 15306.
[5] R. Balog, M. Andersen, B. Jørgensen, Z. Sljivancanin, B. Hammer, A. Baraldi, R. Larciprete, P. Hofmann, L. Hornekær, S. Lizzit, ACS Nano 7 (2013) 3823.
[6] J.H. Jørgensen, A.G. Čabo, R. Balog, L. Kyhl, M.N. Groves, A.M. Cassidy, A. Bruix, M. Bianchi, M. Dendzik, M.A. Arman, L. Lammich, J.I. Pascual, J. Knudsen, B. Hammer, P. Hofmann, L. Hornekær, ACS Nano 10 (2016) 10798.
[7] J.J. Navarro, S. Leret, F. Calleja, D. Stradi, A. Black, R. Bernardo-Gavito, M. Garnica, D. Granados, A.L. Vázquez de Parga, E.M. Pérez, R. Miranda, Nano Lett. 16 (2016) 355.
[8] J.J. Navarro, F. Calleja, R. Miranda, E.M. Pérez, A.L. Vázquez de Parga, Chem. Commun. 53 (2017) 10418–10421.
[9] L. Kyhl, R. Bisson, R. Balog, M.N. Groves, E.L. Kolsbjerg, A.M. Cassidy, J.H. Jørgensen, S. Halkjær, J.A. Miwa, A.G. Čabo, T. Angot, P. Hofmann, M.A. Arman, S. Urpelainen, P. Lacovig, L. Bignardi, H. Bluhm, J. Knudsen,

B. Hammer, L. Hornekær, ACS Nano 12 (2018) 513–520.
[10] C. Romero-Muñiz, A. Martín-Recio, P. Pou, J.M. Gómez-Rodríguez, R. Pérez, Phys. Chem. Chem. Phys. 20 (2018) 19492.
[11] R. Balog, B. Jørgensen, L. Nilsson, M. Andersen, E. Rienks, M. Bianchi, M. Fanetti, E. Lægsgaard, A. Baraldi, S. Lizzit, Z. Sljivancanin, F. Besenbacher, B. Hammer, T.G. Pedersen, P. Hofmann, L. Hornekær, Nat. Mater. 9 (2010) 315.
[12] J. Greenwood, T.H. Phan, Y. Fujita, Z. Li, O. Ivasenko, W. Vanderlinden, H. Van Gorp, W. Frederickx, G. Lu, K. Tahara, Y. Tobe, H. Uji-i, S.F.L. Mertens, S. De Feyter, ACS Nano 9 (2015) 5520–5535.
[13] D. Voiry, A. Goswami, R. Kappera, C.C.C. Silva, D. Kaplan, T. Fujita, M. Chen, T. Asefa, M. Chhowalla, Nat. Chem. 7 (2015) 45.
[14] L. Camilli, J.H. Jørgensen, J. Tersoff, A.C. Stoot, R. Balog, A. Cassidy, J.T. Sadowski, P. Bøggild, L. Hornekær, Nat. Commun. 8 (2017) 47.
[15] J. Tuček, P. Błoński, J. Ugolotti, A.K. Swain, T. Enoki, R. Zbořil, Chem. Soc. Rev. 47 (2018) 3899–3990.
[16] M. Weser, Y. Rehder, K. Horn, M. Sicot, M. Fonin, A.B. Preobrajenski, E.N. Voloshina, E. Goering, Y.S. Dedkov, Appl. Phys. Lett. 96 (2010), 012504.
[17] Y.S. Dedkov, M. Fonin, New J. Phys. 12 (2010) 125004.
[18] R. Decker, J. Brede, N. Atodiresei, V. Caciuc, S. Blügel, R. Wiesendanger, Phys. Rev. B 87 (2013), 041403.
[19] F. Huttmann, D. Klar, N. Atodiresei, C. Schmitz-Antoniak, A. Smekhova, A.J. Martínez-Galera, V. Caciuc, G. Bihlmayer, S. Blügel, T. Michely, H. Wende, Phys. Rev. B 95 (2017), 075427.
[20] A.V. Krasheninnikov, P.O. Lehtinen, A.S. Foster, P. Pyykkö, R.M. Nieminen, Phys. Rev. Lett. 102 (2009) 126807.
[21] O.V. Yazyev, L. Helm, Phys. Rev. B 75 (2007) 125408.
[22] M.M. Ugeda, I. Brihuega, F. Guinea, J.M. Gómez-Rodríguez, Phys. Rev. Lett. 104 (2010), 096804.
[23] R.R. Nair, I.-L. Tsai, M. Sepioni, O. Lehtinen, J. Keinonen, A.V. Krasheninnikov, A.H. Castro Neto, M.I. Katsnelson, A.K. Geim, I.V. Grigorieva, Nat. Commun. 4 (2013) 2010.
[24] J.J. Palacios, J. Fernández-Rossier, L. Brey, Phys. Rev. B 77 (2008) 195428.
[25] O.V. Yazyev, Rep. Prog. Phys. 73 (2010), 056501.
[26] J.J. Palacios, F. Ynduráin, Phys. Rev. B 85 (2012) 245443.
[27] E.J.G. Santos, S. Riikonen, D. Sánchez-Portal, A. Ayuela, J. Phys. Chem. C 116 (2012) 7602–7606.
[28] L. Rodrigo, P. Pou, R. Pérez, Carbon 103 (2016) 200.
[29] C. Ronchi, M. Datteo, D. Perilli, L. Ferrighi, G. Fazio, D. Selli, C. Di Valentin, J. Phys. Chem. C 121 (2017) 8653–8661.
[30] E.J.G. Santos, A. Ayuela, D. Sánchez-Portal, New J. Phys. 14 (2012), 043022.
[31] H.Y. Liu, Z.F. Hou, C.H. Hu, Y. Yang, Z.Z. Zhu, J. Phys. Chem. C 116 (2012) 18193–18201.
[32] J. Nokelainen, I.V. Rozhansky, B. Barbiellini, E. Lähderanta, K. Pussi, Phys. Rev. B 99 (2019), 035441.
[33] H. González-Herrero, J.M. Gómez-Rodríguez, P. Mallet, M. Moaied, J.J. Palacios, C. Salgado, M.M. Ugeda, J.-Y. Veuillen, F. Yndurain, I. Brihuega, Science 352 (2016) 437–441.
[34] D. Geng, Y. Chen, Y. Chen, Y. Li, R. Li, X. Sun, S. Ye, S. Knights, Energy Environ. Sci. 4 (2011) 760.
[35] L. Qu, Y. Liu, J.-B. Baek, L. Dai, ACS Nano 4 (2010) 1321.
[36] X.-K. Kong, C.-L. Chen, Q.-W. Chen, Chem. Soc. Rev. 43 (2014) 2841–2857.
[37] C. Rizescu, I. Podolean, J. Albero, V.I. Parvulescu, S.M. Coman, C. Bucur, M. Puche, H. García, Green Chem. 19 (2017) 1999–2005.
[38] S. Zhou, N. Liu, Z. Wang, J. Zhao, ACS Appl. Mater. Interfaces 9 (2017) 22578–22587.
[39] M. Telychko, P. Mutombo, M. Ondráček, P. Hapala, F.C. Bocquet, J. Kolorenč, M. Vondrávek, P. Jelínek, M. Švec, ACS Nano 8 (2014) 7318.
[40] M. Telychko, P. Mutombo, P. Merino, P. Hapala, M. Ondráček, F.C. Bocquet, J. Sforzini, O. Stetsovych, M. Vondráček, P. Jelínek, M. Švec, ACS Nano 9 (2015) 9180–9187.
[41] A. Martín-Recio, C. Romero-Muñiz, P. Pou, R. Pérez, J.M. Gómez-Rodríguez, Nanoscale 8 (2016) 17686.
[42] X. Fei, J. Neilson, Y. Li, V. Lopez, S.J. Garrett, L. Gan, H.-J. Gao, L. Gao, Nano Lett. 17 (2017) 2887–2894.
[43] A. Martín-Recio, C. Romero-Muñiz, P. Pou, R. Pérez, J.M. Gómez-Rodríguez, Carbon 130 (2018) 362–368.
[44] S. Kawai, S. Saito, S. Osumi, S. Yamaguchi, A.S. Foster, P. Spijker, E. Meyer, Nat. Commun. 6 (2015) 8098.
[45] L. Talirz, P. Ruffieux, R. Fasel, Adv. Mater. 28 (2016) 6222–6231.
[46] M. Stępień, E. Gońka, M. Zyła, N. Sprutta, Chem. Rev. 117 (2017) 3479–3716.
[47] V.D. Pham, J. Lagoute, O. Mouhoub, F. Joucken, V. Repain, C. Chacon, A. Bellec, Y. Girard, S. Rousset, ACS Nano 8 (2014) 9403–9409.
[48] B. de la Torre, M. Švec, P. Hapala, J. Redondo, O. Krejcí, R. Lo, D. Manna, A. Sarmah, D. Nachtigallová, J. Tucek, P. Blonski, M. Otyepka, R. Zboril, P. Hobza, P. Jelínek, Nat. Commun. 9 (2018) 2831.
[49] H.J. Yan, B. Xu, S.Q. Shi, C.Y. Ouyang, J. Appl. Phys. 112 (2012) 104316.
[50] F. Studt, Catal. Lett. 143 (2013) 58–60.
[51] M. Scardamaglia, T. Susi, C. Struzzi, R. Snyders, G. Di Santo, L. Petaccia, C. Bittencourt, Sci. Rep. 7 (2017) 7960.
[52] G. Kresse, J. Furthmüller, Phys. Rev. B 54 (1996) 11169.
[53] G. Kresse, D. Joubert, Phys. Rev. B 59 (1999) 1758.
[54] P.E. Blöchl, Phys. Rev. B 50 (1994) 17953.
[55] J.P. Perdew, K. Burke, M. Ernzerhof, Phys. Rev. Lett. 77 (1996) 3865.
[56] S. Grimme, J. Comput. Chem. 27 (2006) 1787–1799.
[57] A.H. Castro Neto, F. Guinea, N.M.R. Peres, K.S. Novoselov, A.K. Geim, Rev. Mod. Phys. 81 (2009) 109.
[58] F.A. Cotton, G. Wilkinson, Advanced Inorganic Chemistry, fifth ed., John Wiley & Sons, 1988.
[59] H.J. Monkhorst, J.D. Pack, Phys. Rev. B 13 (1976) 5188.
[60] M. Methfessel, A.T. Paxton, Phys. Rev. B 40 (1989) 3616.
[61] G. Henkelman, A. Arnaldsson, H. Jónsson, Comput. Mater. Sci. 36 (2006) 354–360.
[62] E. Sanville, S.D. Kenny, R. Smith, G. Henkelman, J. Comput. Chem. 28 (2007) 899–908.
[63] W. Tang, E. Sanville, G. Henkelman, J. Phys. Condens. Matter 21 (2009), 084204.
[64] J. Tersoff, D.R. Hamann, Phys. Rev. Lett. 50 (1983) 1998.
[65] J. Tersoff, D.R. Hamann, Phys. Rev. B 31 (1985) 805.
[66] I. Horcas, R. Fernández, J.M. Gómez-Rodríguez, J. Colchero, J. Gómez-Herrero, A.M. Baró, Rev. Sci. Instrum. 78 (2007), 013705.
[67] A.M. Suarez, L.R. Radovic, E. Bar-Ziv, J.O. Sofo, Phys. Rev. Lett. 106 (2011) 146802.
[68] Y. Dai, S. Ni, Z. Li, J. Yang, J. Phys. Condens. Matter 25 (2013) 405301.
[69] T. Sun, X. Yao, S. Fabris, J. Phys. Chem. A 120 (2016) 2607–2613.
[70] Ž. Šljivančanin, A.S. Milošević, Z.S. Popović, F.R. Vukajlović, Carbon 54 (2013) 482–488.
[71] F. Mehmood, R. Pachter, W. Lu, J.J. Boeckl, J. Phys. Chem. C 117 (2013) 10366–10374.
[72] E.H. Lieb, Phys. Rev. Lett. 62 (1989) 1201.
[73] P. Błoński, J. Tuček, Z. Sofer, V. Mazánek, M. Petr, M. Pumera, M. Otyepka, R. Zbořil, J. Am. Chem. Soc. 139 (2017) 3171–3180.
[74] J. Tuček, P. Błoński, Z. Sofer, P. Šimek, M. Petr, M. Pumera, M. Otyepka, R. Zbořil, Adv. Mater. 28 (2016) 5045–5053.
[75] N.T.T. Tran, D.K. Nguyen, O.E. Glukhova, M.-F. Lin, Sci. Rep. 7 (2017) 17858.
[76] F. Marsusi, N. Drummond, M. Verstraete, Carbon 144 (2019) 615–627.
[77] N.A. Vinogradov, K. Schulte, M.L. Ng, A. Mikkelsen, E. Lundgren, N. Mårtensson, A.B. Preobrajenski, J. Phys. Chem. C 115 (2011) 9568.
[78] M. Yi, W. Zhang, Z. Shen, X. Zhang, X. Zhao, Y. Zheng, S. Ma, J. Nanoparticle Res. 15 (2013) 1811.